Electronic Supplementary Material (ESI) for Dalton Transactions.

Antenna triplet DFT calculations to drive the design of luminescent Ln^{3+} complexes.

Luca Babetto,[a] Silvia Carlotto[a,b*] Alice Carlotto,[a] Marzio Rancan,[b] Gregorio Bottaro,[b] Lidia Armelao[a,b] and Maurizio Casarin[a,b*]

[a]Dipartimento di Scienze Chimiche, Università degli Studi di Padova, via F. Marzolo 1, 35131 Padova, Italy.

[b] Institute of Condensed Matter Chemistry and Technologies for Energy (ICMATE), National Research Council (CNR), c/o Department of Chemistry, University of Padova, via F. Marzolo 1, 35131 Padova, Italy

1. ANTENNA EFFECT

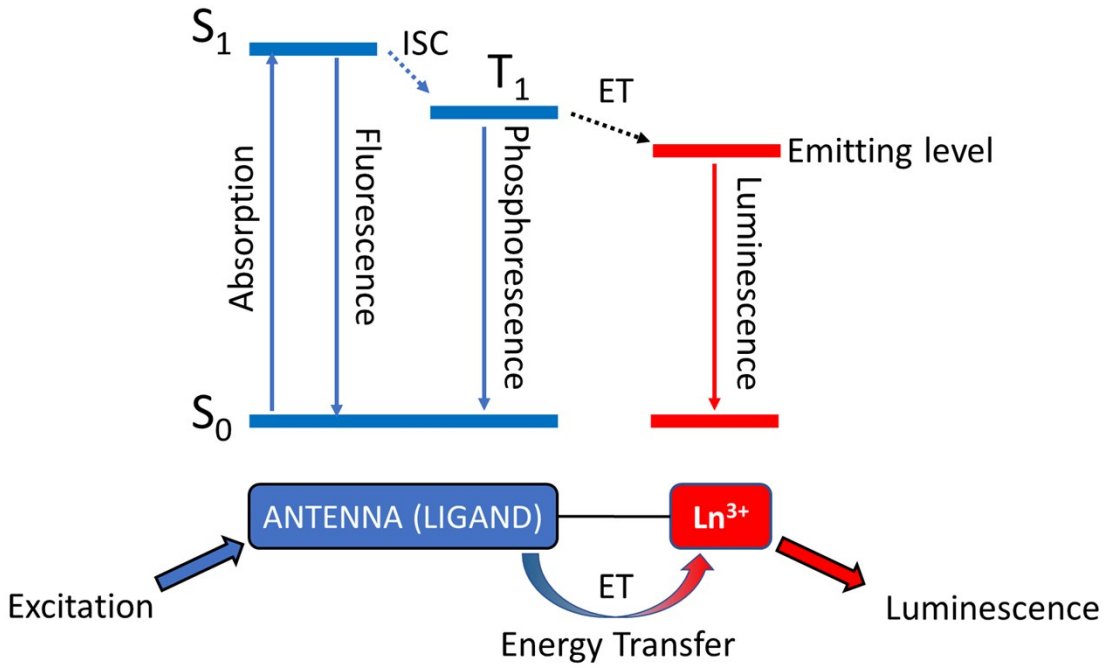

Figure S1. Energy level diagram illustrating the antenna effect. In blue the antenna processes and in red the Ln^{3+} one. ISC is the intersystem crossing process. S and T designates levels with singlet and triplet multiplicity, respectively.

2. SYNTHESES

Reagents were purchased from Aldrich and used as received. The elemental analyses were carried out with a Flash 2000 Thermo Scientific Analyzer at the Department of Chemical Sciences of the University of Padova.

Syntheses of L1 and L2. The ligands 1-(naphthalen-3-yl)-3-(thiophen-2-yl)propane-1,3-dione (**L1**) and 1-(phenanthren-3-yl)-3-(thiophen-2-yl)propane-1,3-dione (**L2**) were synthesized and characterized as reported in literature.[1]

Synthesis of (2Z)-3-hydroxy-3-(pyren-1-yl)-1-(thiophen-2-yl)prop-2-en-1-one (L3). The Claisen condensation was performed under argon in dry THF. Potassium *tert*-butoxide (1.12 g, 10 mmol) was added to a THF (22 ml) solution of 1-acetylpyrene (1.85 g, 7.5 mmol) and ethyl-2-thiophenecarboxylate (1.74 g, 11 mmol). The resulting solution turned to dark-red and was stirred for 18 days at 40-50°C. After cooling, the crude was acidified with 30 ml of 10% HCl. The product was extracted with dichloromethane to give a red-brown solution and dried over $MgSO_4$. The crude product was purified by recrystallization (6 times) from DCM/hexane (1:3). Yield: 48%.
ESI-MS (negative ions, MeOH): *m/z* 353.23 $[L3\text{-}H]^-$

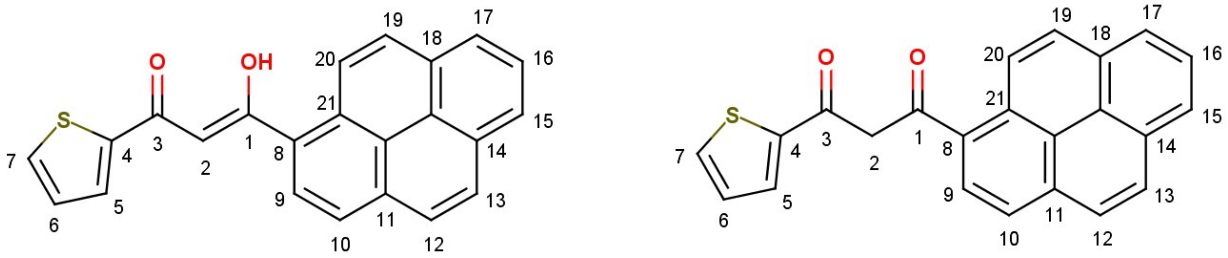

Figure S2. Ligand **L3**, keto enol (left) and diketone (right) tautomers.

^{1}H NMR ($CDCl_3$, 400 MHz, T = 25 °C) Keto enol tautomer (~96%), δ [ppm] = 6.69 (1H, s, H_2), 7.17 (1H, dd, $^3J_{H6,H7}$ = 5.1 Hz, $^3J_{H6,H5}$ = 3.9 Hz, H_6), 7.65 (1H, dd, $^3J_{H7,H6}$ = 5.0 Hz, $^4J_{H7,H5}$ = 1.1 Hz, H_7), 7.81 (1H, dd, $^3J_{H5,H6}$ = 3.9 Hz, $^4J_{H5,H7}$ = 1.1 Hz, H_5) 7.99-8.32 (ov, 8H, m, H_{10}, H_{12}, H_{13}, H_{15}, H_{16}, H_{17}, H_{19}, H_{20}), 8.79 (1H, d, $^3J_{H20,H19}$ = 9.2 Hz, H_9), 16.55 (1H, s, OH). Diketone tautomer (~4%), δ [ppm] = 4.83 (2H, s, H_2), 7.13 (1H, dd, $^3J_{H6,H7}$ = 5.0 Hz, $^3J_{H6,H5}$ = 3.8 Hz, H_6), 7.63 (1H, dd, $^3J_{H7,H6}$ = 5.0 Hz, $^4J_{H7,H5}$ = 1.2 Hz, H_7), 7.88 (1H, dd, $^3J_{H5,H6}$ = 3.8 Hz, $^4J_{H5,H7}$ = 1.2 Hz, H_5) 7.99-8.34 (ov, 9H, m, H_9, H_{10}, H_{12}, H_{13}, H_{15}, H_{16}, H_{17}, H_{19}, H_{20}).
^{13}C-NMR ($CDCl_3$, 100 MHz, T = 25 °C) Keto enol tautomer δ [ppm] = 99.33, 124.83, 124.99, 126.30, 126.46, 126.53, 126.73, 127.54, 128.74, 129.26, 129.52, 130.89, 133.12 (*C*H), 124.80, 125.26, 129.41, 130.66, 130.98, 131.52, 133.64, 142.30 (*C*), 182.37, 185.51 (*C*=O, *C*-OH)

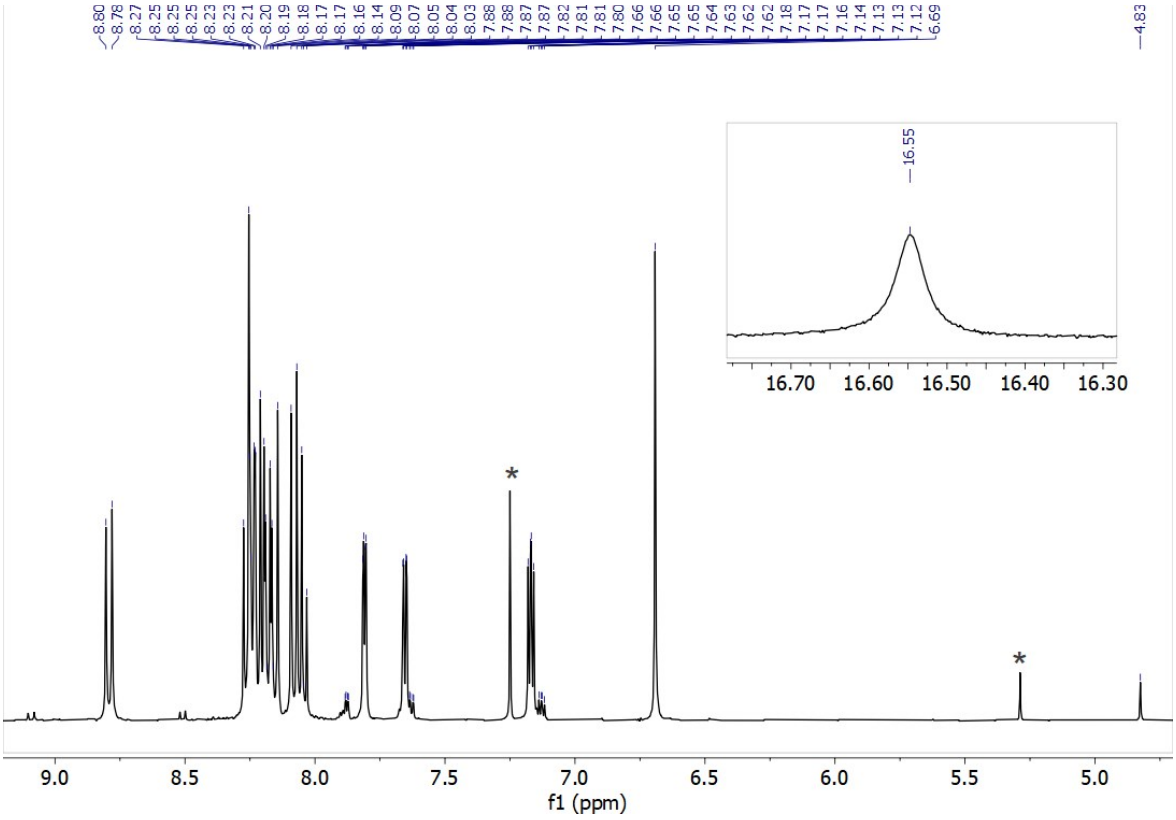

Figure S3. ^{1}H-NMR of ligand **L3** in $CDCl_3$. Inset: OH signal. Solvent signals are marked with an asterisk.

2.2 Complexes syntheses.

Synthesis of [Gd(L3)$_3$(EtOH)$_2$] (Gd3). An ethanol solution (2.5 ml) of $Gd(NO_3)_3 \cdot 6H_2O$ (32.6 mg, 0.07 mmol) was added dropwise to a hot ethanol solution (3.5 ml) of **L3** (77.4 mg, 0.22 mmol) and TEAOH solution 25 % wt (170 µl, 0.26 mmol). A yellow powder precipitated, the mixture was stirred and heated at 75 °C for overnight. The yellow powder was recovered by centrifugation and washed with cold EtOH. Yield: 60 %. LDI-MS (positive ions): *m/z* 1256.43 [Gd(**L3**)$_3$+K]$^+$, 1240.49 [Gd(**L3**)$_3$+Na]$^+$. Elemental analysis for $GdC_{73}H_{51}O_8S_3$: calculated C 66.95 %, H 3.93 %, S 7.35 %; found: C 67.02 %, H 3.99 %, S 7.42 %.

3. MASS SPECTROMETRY ANALYSIS

Electrospray mass spectrometric measurements – instrumental setup

Electrospray mass spectrometric measurements (ESI/MS) were performed using a LCQ Fleet ion trap instrument (ThermoFisher), operating in negative ion mode. The entrance capillary temperature and voltage were 280°C and 4 kV, respectively. Sample (**L3**) solutions (10^{-6} M in methanol) was introduced by direct infusion using a syringe pump at a flow rate of 8 µL×min^{-1}.

LDI mass spectrometric measurements – instrumental setup

LDI/MS measurements were performed using a MALDI/TOF/TOF UltrafleXtreme instrument (Bruker Daltonics, Bremen, Germany), equipped with a 1 kHz smartbeam II laser (λ= 355 nm) and operating in the reflectron positive ion mode. The instrumental conditions were: IS1 = 25 kV; IS2 = 22.4 kV; reflectron potential = 26.3 kV; delay time = 120 nsec.

External mass calibration (Peptide Calibration Standard) was based on monoisotopic values of [M+H]$^+$ of angiotensin II, angiotensin I, substance P, bombesin, ACTH clip (1-17), ACTH clip (18-39), somatostatin 28 at m/z 1046.5420, 1296.6853, 1347.7361, 1619.8230, 2093.0868, 2465.1990 and 3147.4714, respectively.

1 mL of acetonitrile (**Gd3**) sample solution was deposited on the stainless-steel sample holder and allowed to dry before introducing into the mass spectrometer.

4. SINGLE CRYSTAL X-RAY DIFFRACTION

Mo Kα (λ = 0.71073 Å) radiation was used for **L1** and Cu Kα (λ = 1.54184 Å) for **L2** and **L3** . Data were collected at room temperature by means of the ω - scans technique using graphite–monochromated radiation. The diffraction intensities were corrected for Lorentz and polarization effects and were also optimized with respect to absorption. Empirical multi–scan absorption corrections using equivalent reflections were performed with the scaling algorithm SCALE3 ABSPACK. Data collection, data reduction and finalization were carried out through the CrysAlisPro software. Structures were solved with the ShelXT[2] program by Intrinsic Phasing and refined with the ShelXL[3] package using least squares minimisation, in the framework of Olex2 software.[4] In the last cycles of refinement, non-hydrogen atoms were refined anisotropically.

L1 was tretated as an inversion twin with TWIN instruction of SHELX was applied (BASF 0.2). For **L2** and **L3** in the thienyl moiejty the rotation of the ring by 180° could not be negletted. These fragments were splitted in two parts the occupancies of which were constrained to sum to 1. DFIX, SADI and FLAT restrains have been applied to better model the fragments. EADP constrain has been applied to selected atoms. Crystallographic data and refining details are aviable in Table S1 in the CIF files deposited with the Cambridge Crystallographic Data Centre as supplementary publication (CCDC 1998680-1998682).

Table S1. Crystal data and structure refinement for **L1**, **L2** and **L3.**

Identification code	**L1**	**L2**	**L3**
Empirical formula	$C_{17}H_{12}O_2S$	$C_{21}H_{14}O_2S$	$C_{23}H_{14}O_2S$
Formula weight	280.33	330.38	354.40
Temperature/K	299.3(2)	297.3(5)	297.6(6)
Crystal system	orthorhombic	orthorhombic	triclinic

Space group	$Pca2_1$	$P2_12_12_1$	P-1
a/Å	8.7457(4)	6.32131(13)	9.1371(3)
b/Å	6.3938(2)	12.7658(3)	10.1916(3)
c/Å	23.9293(9)	20.1479(5)	10.4736(3)
α/°	90	90	78.929(3)
β/°	90	90	65.508(3)
γ/°	90	90	71.717(3)
Volume/Å^3	1338.08(9)	1625.87(6)	840.58(5)
Z	4	4	2
ρ_{calc}g/cm^3	1.392	1.350	1.400
μ/mm^{-1}	0.239	1.839	1.821
F(000)	584.0	688.0	368.0
Crystal size/mm^3	0.3 × 0.25 × 0.15	0.35 × 0.23 × 0.02	0.3 × 0.2 × 0.15
Radiation	MoKα (λ = 0.71073)	CuKα (λ = 1.54184)	CuKα (λ = 1.54184)
2Θ range for data collection/°	6.372 to 56.56	8.2 to 145.486	9.162 to 145.616
Index ranges	-11 ≤ h ≤ 11, -8 ≤ k ≤ 8, -31 ≤ l ≤ 31	-7 ≤ h ≤ 7, -15 ≤ k ≤ 15, -24 ≤ l ≤ 24	-10 ≤ h ≤ 11, -12 ≤ k ≤ 12, -12 ≤ l ≤ 12
Reflections collected	15330	13259	9770
Independent reflections	3308 [R_{int} = 0.0219, R_{sigma} = 0.0170]	3233 [R_{int} = 0.0241, R_{sigma} = 0.0209]	3339 [R_{int} = 0.0193, R_{sigma} = 0.0217]
Data/restraints/parameters	3308/1/183	3233/28/226	3339/54/255
Goodness-of-fit on F^2	1.068	1.042	1.062
Final R indexes [I≥2σ (I)]	R_1 = 0.0329, wR_2 = 0.0876	R_1 = 0.0358, wR_2 = 0.0993	R_1 = 0.0433, wR_2 = 0.1276
Final R indexes [all data]	R_1 = 0.0357, wR_2 = 0.0899	R_1 = 0.0387, wR_2 = 0.1022	R_1 = 0.0486, wR_2 = 0.1344
Largest diff. peak/hole / e Å^{-3}	0.18/-0.21	0.17/-0.20	0.21/-0.18
Flack parameter	Inversion Twin (BASF 0.2)	0.014(9)	---
CCDC	1998680	1998681	1998682

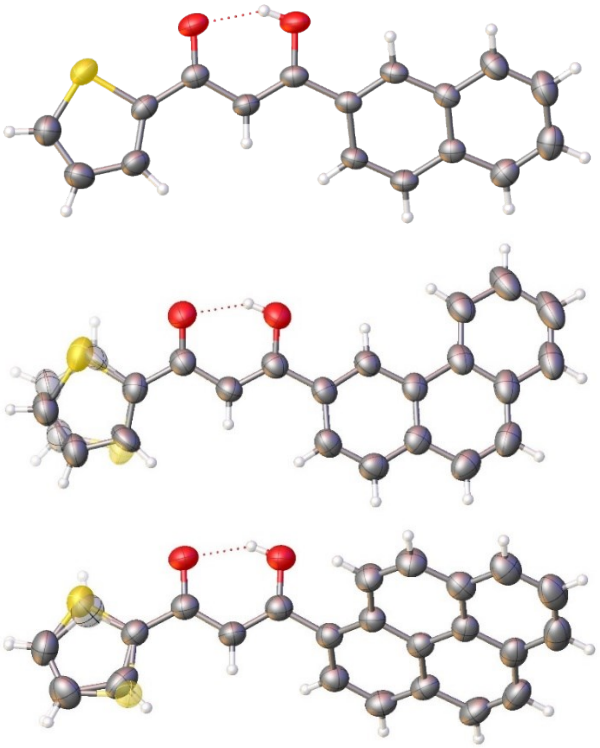

Figure S4. SCXRD structure of **L1** (a), **L2** (b) and **L3** (c). Colour code: C grey, O red, S yellow. Thermal ellipsoids are drawn at the 50% probability level. Disordered parts translucent.

5. LIGAND GEOMETRIES

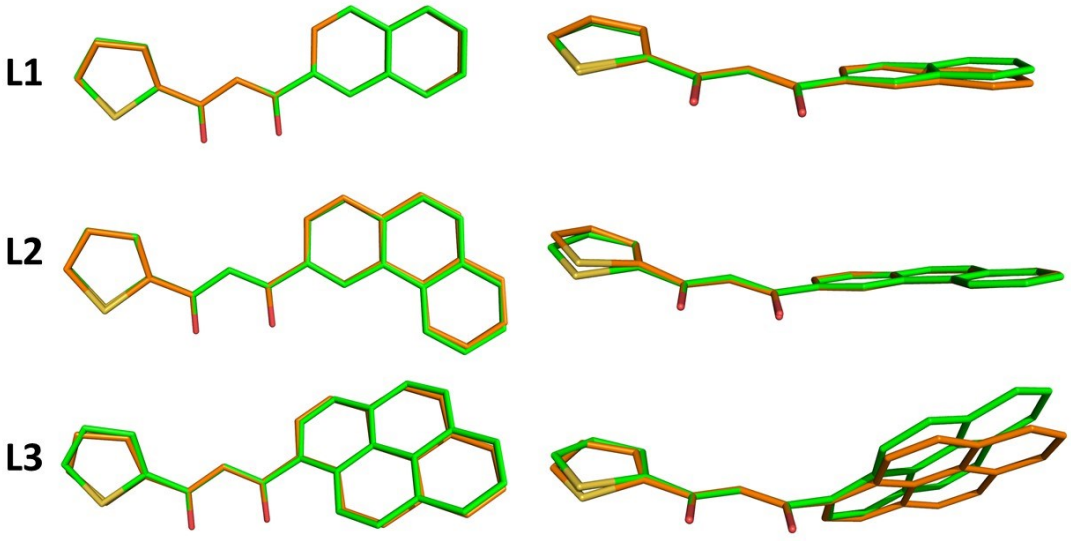

Figure S5. Comparison between the B3LYP (green) and experimental (orange) structures of the ligands.

Table S2. Theoretical abundance of the diverse rotamers in **L1**, **L2**, and **L3** in toluene. The energy differences (kcal/mol) with respect to the most stable rotamer are reported in parentheses.

	A	B	C	D
L1	61%	12% (+0.96)	21% (+0.62)	5% (+1.43)
L2	62%	17% (+0.77)	17% (+0.78)	4% (+1.56)
L3	33% (+0.25)	7% (+1.15)	50%	10% (+0.95)

Table S3. Theoretical abundance of the diverse rotamers in **L1**, **L2**, and **L3** with the inclusion of dispersion corrections in vacuum. The energy differences (kcal/mol) with respect to the most stable rotamer are reported in parentheses.

	A	B	C	D
L1	51%	21% (+0.53)	19% (+0.59)	10% (+0.97)
L2	42%	26% (+0.28)	21% (+0.41)	11% (+0.78)
L3	13% (+0.94)	5% (+1.47)	62%	21% (+0.65)

6. UV-VIS ABSORPTION AND PHOTOLUMINESCENCE SPECTROSCOPIES

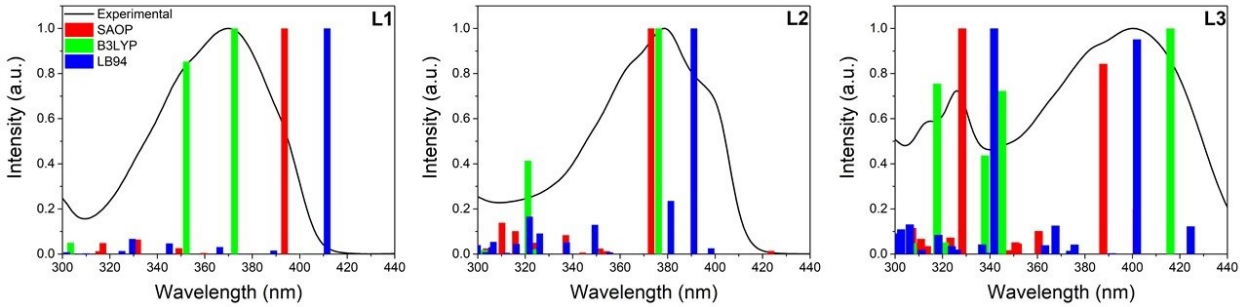

Figure S6. Comparison between calculated vertical excitation energies on the rotamer A for **L1** (a), **L2** (b) and **L3** (c) with different functionals (SAOP, LB94, B3LYP). The ground state geometries have been optimized at B3LYP level of theory.

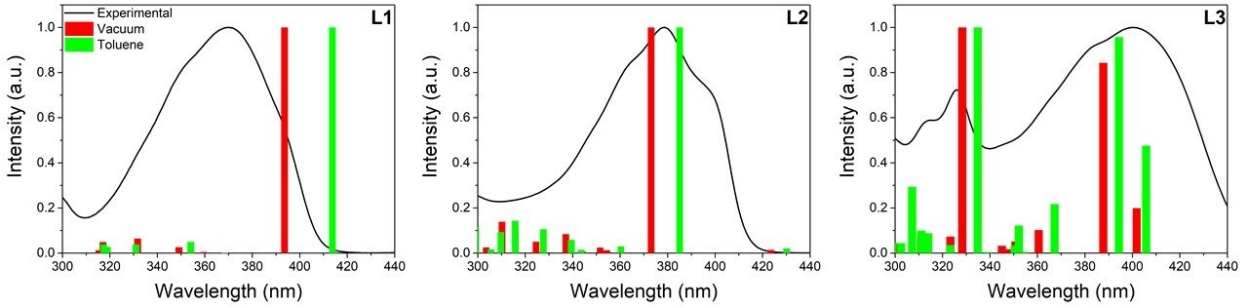

Figure S7. Comparison between calculated vertical excitation energies on the rotamer A for **L1** (a), **L2** (b) and **L3** (c) with SAOP in vacuum and in solvent (toluene). The ground state geometries have been optimized at B3LYP level of theory.

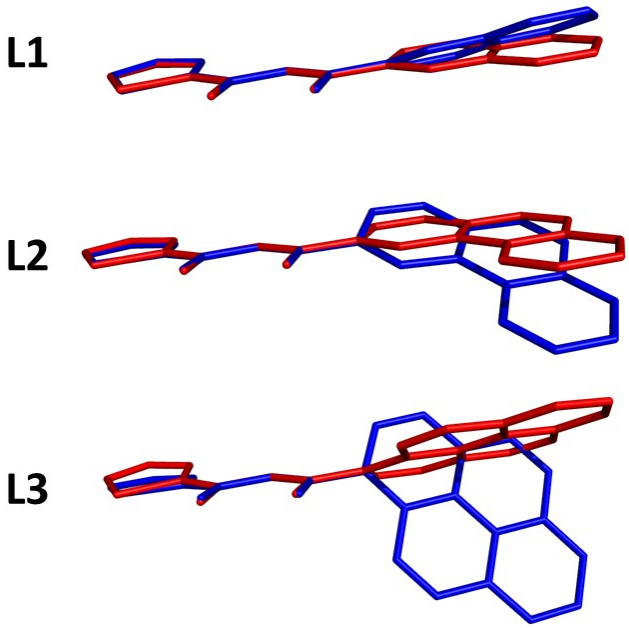

Figure S8. Comparison between the ground state S_0 (blue) and excited singlet state S_1 (red) structures of the ligands **L1**, **L2**, and **L3** calculated at the B3LYP level of theory for rotamer A. For **L3** the calculated Franck-Condon factors are zero due to the significantly different geometries of the two states.

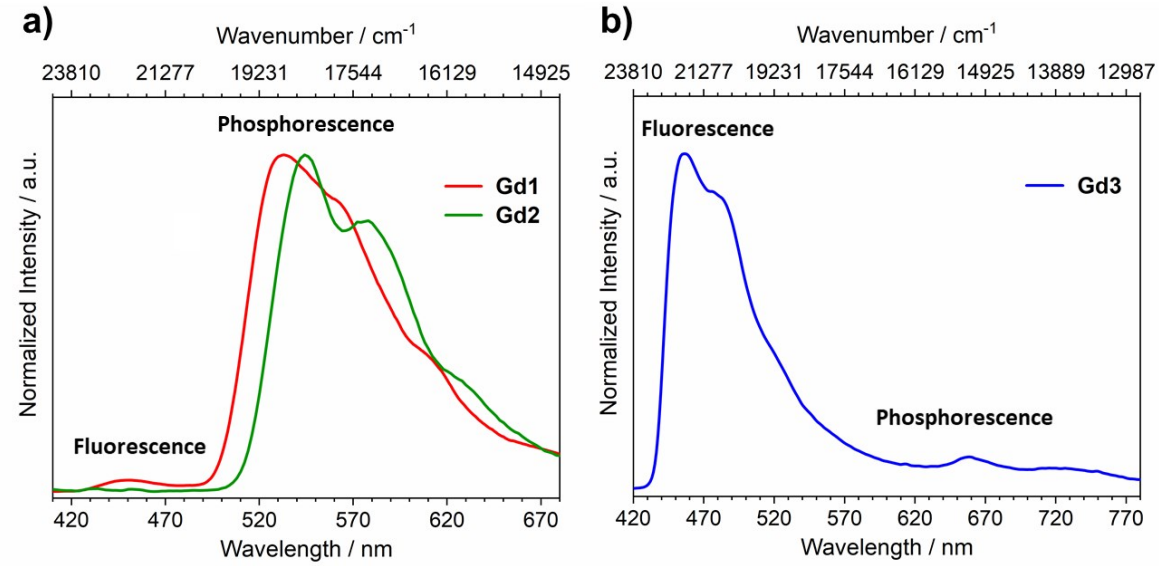

Figure S9. Phosphorescence spectra recorded at 77 K of gadolinium complexes embedded in polystyrene thin film (*ca.* 2 µm thick): a) **Gd1** and **Gd2** with a 300 µs delay after the excitation pulse (λ_{ex} = 370 nm); b) **Gd3** (λ_{ex} = 380 nm) recorded using a continuous light source (Xe lamp). Inset: zoom of the spectrum in the phosphorescence region (610-730 nm).

7. TD-DFT ABSORPTION SPECTRA

Table S4. Most relevant TD-DFT/SAOP UV-Vis electronic transitions for the rotamers A, B, C, and D of ligand **L1**. Intensities are weighted by the relative abundance of the rotamer. Only transitions in the 300 – 480 nm range with normalized intensities higher than 20% of the most intense transition for each form have been included. MO_i and MO_f are the initial and the final MOs involved in the transition. Components accounting for less than 10% are neglected. Graphical representations of the orbitals involved in the predominant transition are reported.

transition	*wavelength (nm)*	*weighted intensity*	$MO_i \longrightarrow MO_f$	MO_i	MO_f
2A	394	0.50	H-1 ⟶ L (52%) H ⟶ L (38%)	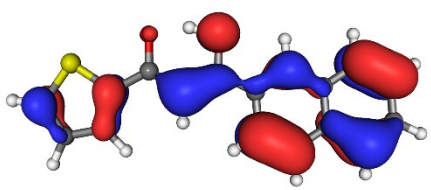	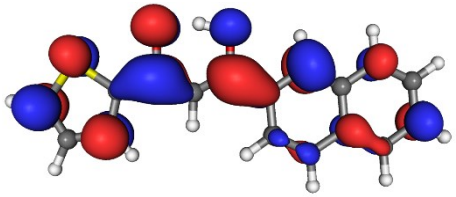
2B	382	0.19	H-1 ⟶ L (63%) H ⟶ L (27%)	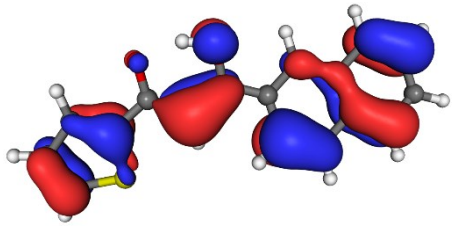	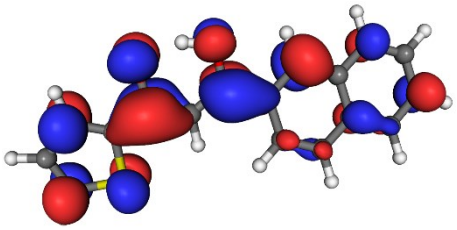
2C	378	0.22	H-1 ⟶ L (62%) H ⟶ L (22%)	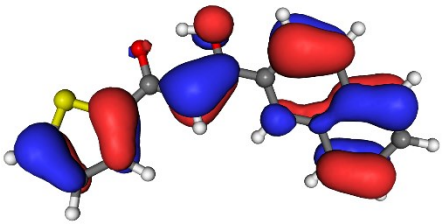	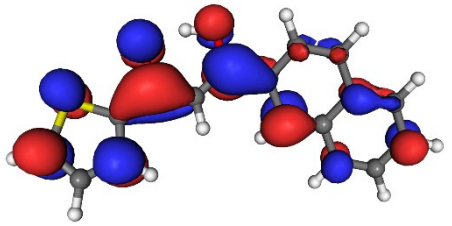
2D	380	0.09	H-1 ⟶ L (66%) H ⟶ L (20%)	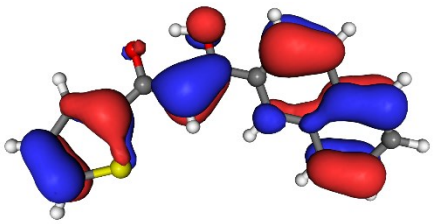	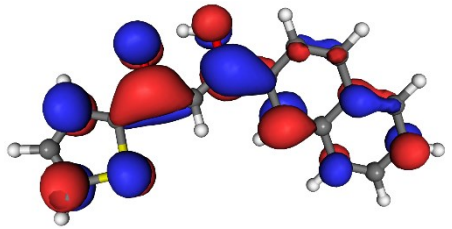

Table S5. Most relevant TD-DFT/SAOP UV-Vis electronic transitions for the rotamers A, B, C, and D of ligand **L2**. Intensities are weighted by the relative abundance of the rotamer. Only transitions in the 300 – 480 nm range with normalized intensities higher than 20% of the most intense transition for each form have been included. MO_i and MO_f are the initial and the final MOs involved in the transition. Components accounting for less than 10% are neglected. Graphical representations of the orbitals involved in the predominant transition are reported.

transition	*wavelength (nm)*	*weighted intensity*	$MO_i \longrightarrow MO_f$	MO_i	MO_f
3A	398	0.49	H-2 ⟶ L (66%) H ⟶ L+1 (12%) H ⟶ L (10%)	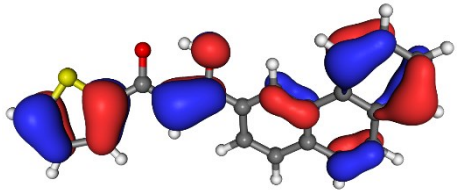	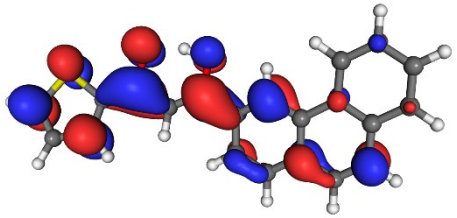
3B	400	0.24	H-2 ⟶ L (70%) H ⟶ L (10%)	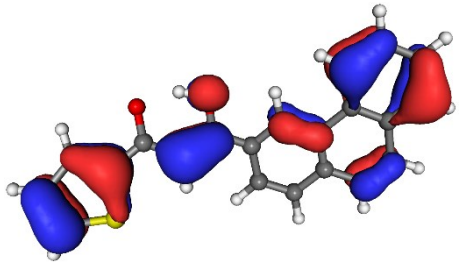	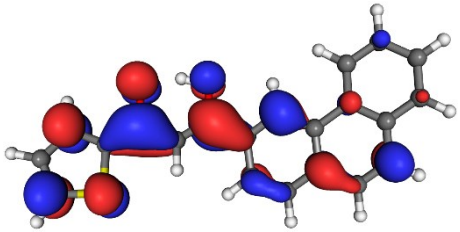
3C	398	0.19	H-2 ⟶ L (66%) H ⟶ L+1 (16%) H ⟶ L (10%)	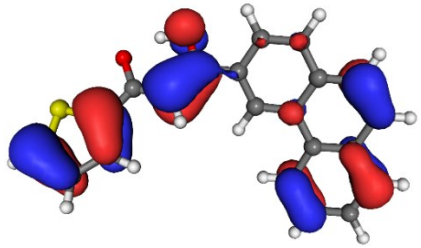	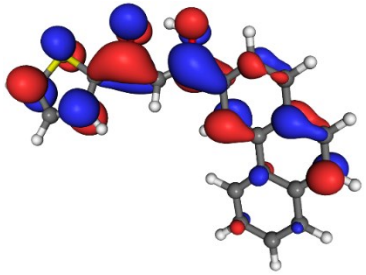
3D	399	0.08	H-2 ⟶ L (70%) H ⟶ L+1 (15%)	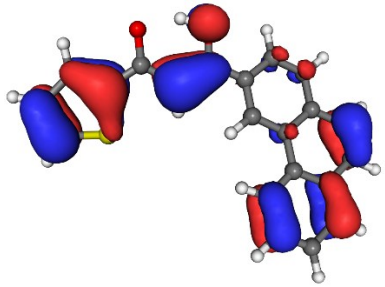	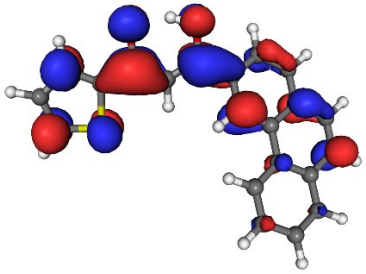

Table S6. Most relevant TD-DFT/SAOP UV-Vis electronic transitions for the rotamers A, B, C, and D of ligand **L3**. Intensities are weighted by the relative abundance of the rotamer. Only transitions in the 300 – 480 nm range with normalized intensities higher than 20% of the most intense transition for each form have been included. MO_i and MO_f are the initial and the final MOs involved in the transition. Components accounting for less than 10% are neglected. Graphical representations of the orbitals involved in the predominant transition are reported.

transition	*wavelength (nm)*	*weighted intensity*	$MO_i \longrightarrow MO_f$	MO_i	MO_f
2A	402	0.05	H-2 ⟶ L (61%) H-1 ⟶ L (28%)	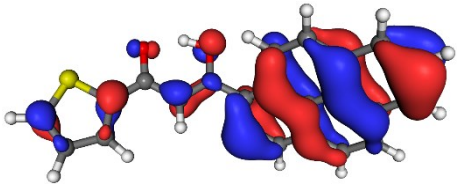	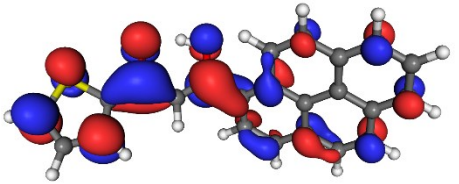
3A	388	0.23	H ⟶ L+1 (37%) H-2 ⟶ L (23%) H-1 ⟶ L (17%) H-1 ⟶ L+1 (13%)	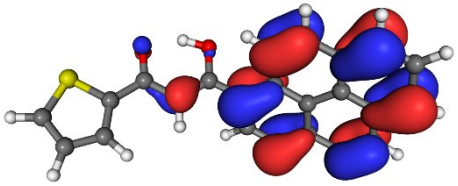	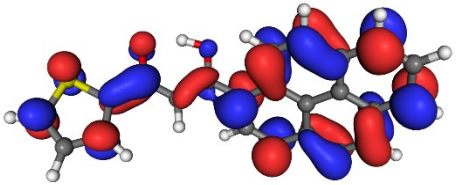
9A	328	0.27	H-1 ⟶ L+1 (28%) H-1 ⟶ L (25%) H-2 ⟶ L+1 (15%) H-6 ⟶ L (11%)	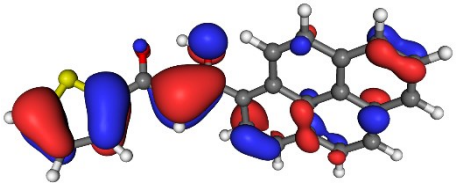	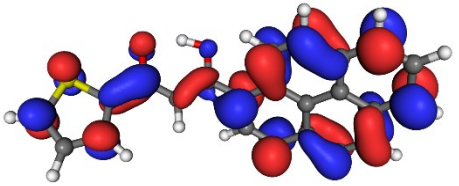
2B	402	0.01	H-2 ⟶ L (48%) H-1 ⟶ L (38%)	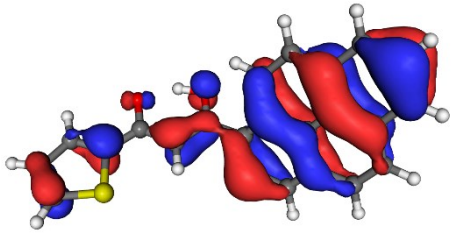	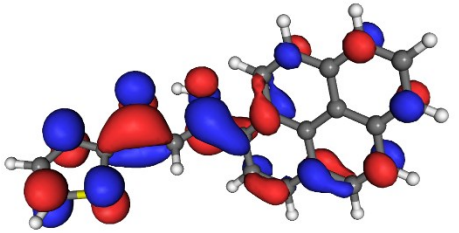

3B	388	0.05	H ⟶ L+1 (37%) H-2 ⟶ L (30%) H-1 ⟶ L (11%) H-1 ⟶ L+1 (10%)	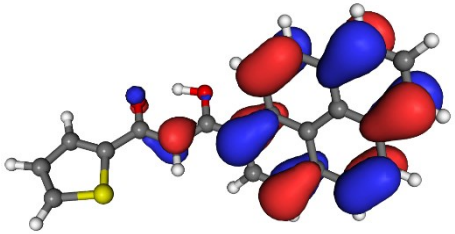	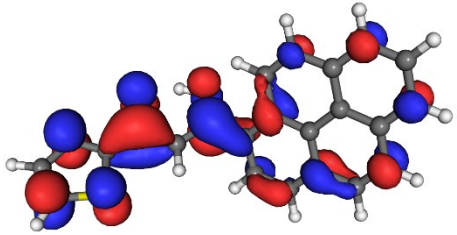
9B	329	0.05	H-1 ⟶ L+1 (30%) H-2 ⟶ L+1 (28%) H-1 ⟶ L (16%)	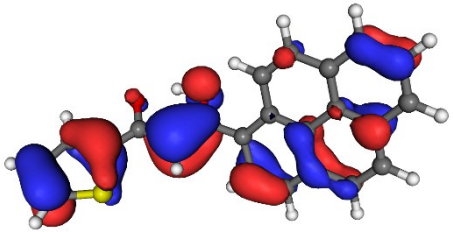	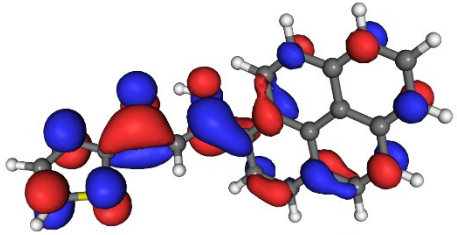
2C	409	0.49	H-1 ⟶ L (64%) H ⟶ L+1 (17%)	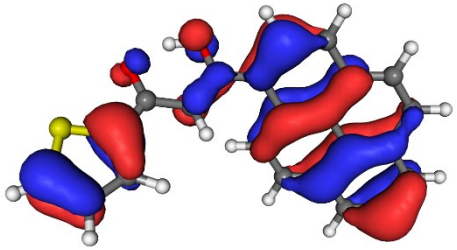	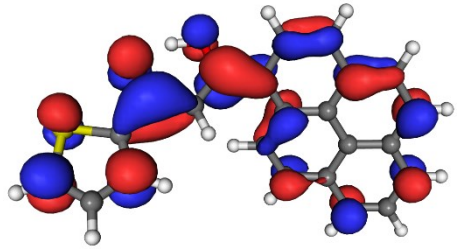
9C	332	0.11	H-5 ⟶ L (59%)	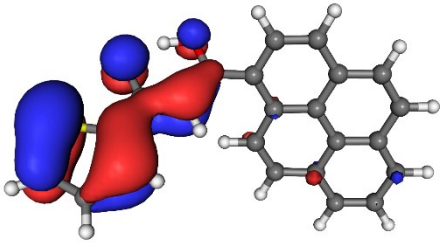	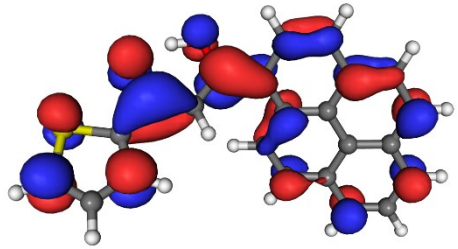
10C	321	0.30	H ⟶ L+3 (39%) H-2 ⟶ L+1 (20%) H-1 ⟶ L+1 (17%)	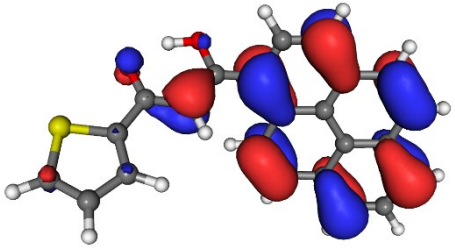	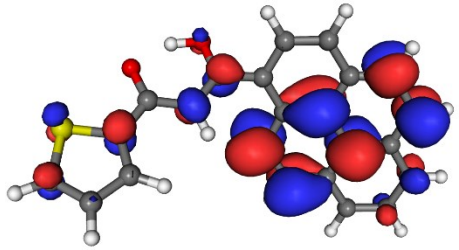

2D	409	0.08	H-1 ⟶ L (66%) H ⟶ L+1 (17%)	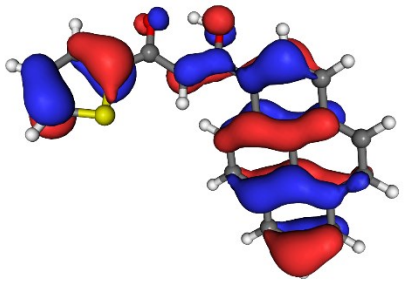	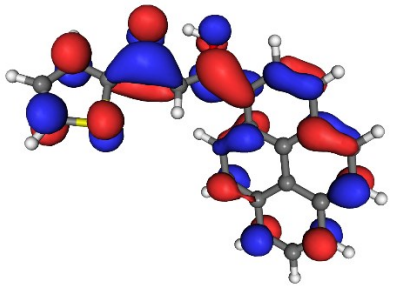
9D	332	0.01	H-5 ⟶ L (54%) H ⟶ L+3 (12%)	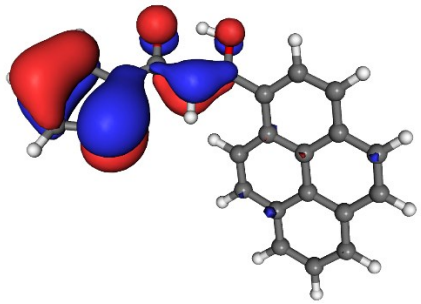	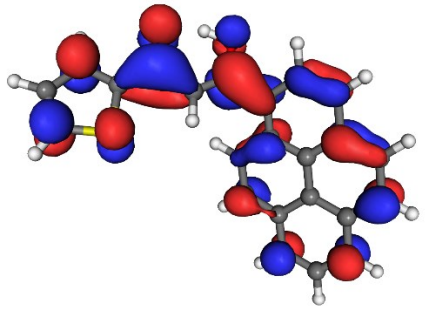
10D	321	0.05	H ⟶ L+3 (32%) H-2 ⟶ L+1 (25%) H-1 ⟶ L+1 (17%)	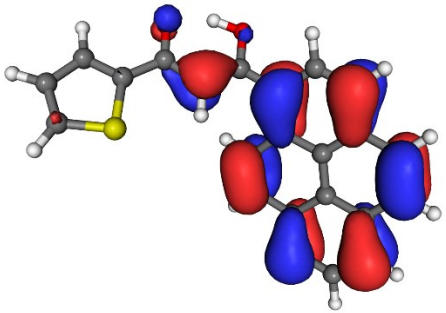	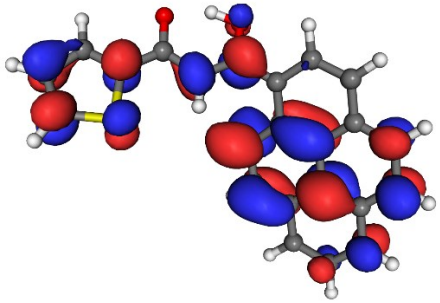

8. REFERENCES

1. Carlotto, A.; Babetto, L.; Carlotto, S.; Miozzi, M.; Seraglia, R.; Casarin, M.; Bottaro, G.; Rancan, M.; Armelao, L., *ChemPhotoChem,* **2020**, *4*, 674–684.
2. G. M. Sheldrick, *Acta Cryst*. **2015**, *A71*, 3.
3. *G. M. Sheldrick, Acta Cryst.* ***2015****, C71, 3.*
4. O. V. Dolomanov, L. J. Bourhis, R. J. Gildea, J. A. K. Howard, H. Puschmann, *J. Appl. Crystallogr.* **2009**, *42*, 339.